Evidence from Opportunity's Microscopic Imager for Water on Meridiani Planum

K. E. Herkenhoff,[1]* S. W. Squyres,[2] R. Arvidson,[3] D. S. Bass,[4] J. F. Bell III,[2] P. Bertelsen,[5] B. L. Ehlmann,[3] W. Farrand,[6] L. Gaddis,[1] R. Greeley,[7] J. Grotzinger,[8] A. G. Hayes,[2] S. F. Hviid,[9] J. R. Johnson,[1] B. Jolliff,[3] K. M. Kinch,[10] A. H. Knoll,[11] M. B. Madsen,[5] J. N. Maki,[4] S. M. McLennan,[12] H. Y. McSween,[13] D. W. Ming,[14] J. W. Rice Jr.,[7] L. Richter,[15] M. Sims,[16] P. H. Smith,[17] L. A. Soderblom,[1] N. Spanovich,[17] R. Sullivan,[2] S. Thompson,[7] T. Wdowiak,[18] C. Weitz,[19] P. Whelley[7]

The Microscopic Imager on the Opportunity rover analyzed textures of soils and rocks at Meridiani Planum at a scale of 31 micrometers per pixel. The uppermost millimeter of some soils is weakly cemented, whereas other soils show little evidence of cohesion. Rock outcrops are laminated on a millimeter scale; image mosaics of cross-stratification suggest that some sediments were deposited by flowing water. Vugs in some outcrop faces are probably molds formed by dissolution of relatively soluble minerals during diagenesis. Microscopic images support the hypothesis that hematite-rich spherules observed in outcrops and soils also formed diagenetically as concretions.

The Athena science payload on the Mars Exploration Rover (MER) mission includes the Microscopic Imager (MI), a camera designed to provide views that are similar to that seen through a geologist's hand lens (*1*, *2*). MI data are acquired in order to place other MER instrument data in context and to aid in petrologic and geologic interpretations of rocks and soils on Mars. The MI on Opportunity is essentially identical to the MI on Spirit and is used in a similar manner (*3*).

During the first 90 sols (*4*) of its surface mission (*5*), the Opportunity rover acquired and returned 870 MI images (including subframes) of rocks, soil/bedform targets, and the martian sky (for calibration). Tracks and trenches created by the rover wheels were also imaged (*6*), as were the filter and capture magnets on the front of the rover (*7*).

MI observations of soil-like materials (*8*) within Eagle crater (*9*) and on the surrounding plains have been used to assess cohesion and cementation of very fine-grained (<125 μm) material, based on soil morphology after disturbances caused by the rover wheels and by the Mössbauer spectrometer (MB) contact plate (*10*). Granules on the surface typically are pressed into the underlying very fine sand by MB contact; cohesion between grains is indicated where this results in very short, near-vertical walls in the surrounding soil (Fig. 1). Some MI observations of soils disturbed by the MB contact plate show apparent fractures, suggesting that cementation of surface particles has formed a crust. The thickness of this crust is estimated to be at least 1 mm (the penetration depth of the MB contact plate) based on images taken after the surface was disrupted (e.g., Fig. 1). Plausibly, and consistent with Alpha Particle X-Ray Spectrometer (APXS) spectra of soil-like deposits at the Meridiani site (*11*), the cementation is caused by precipitation of various salts (e.g., Cl- and SO_4-bearing) that bridge soil particles. Salts in the dust (unresolved by the MI) may dissolve and migrate into voids between soil particles in thin films of water (*12*) adsorbed onto soil particles. Thin liquid films may occur in soils when the spin axis obliquity and atmospheric relative humidity are high enough to cause precipitation or condensation of water. During warming events, salts precipitate on soil particles as thin liquid films evaporate (*13*), weakly cementing the upper soil surface.

In many places, Meridiani soils contain a major, distinctive component in the form of 0.6- to 6-mm-diameter spherules (*14*). These

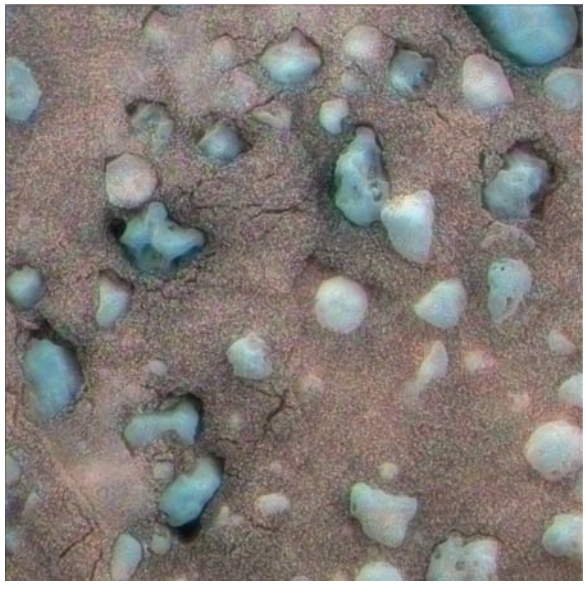

Fig. 1. False-color merge of MI image of target Munter (1M133692453), taken on sol 62, with Pancam multispectral data (effective wavelengths of 602, 535, and 483 nm). The MI image was acquired after MB contact, when the target was in complete shadow. The area shown is 3 cm across.

[1]U.S. Geological Survey Astrogeology Team, Flagstaff, AZ 86001, USA. [2]Department of Astronomy, Space Sciences Building, Cornell University, Ithaca, NY 14853, USA. [3]Department of Earth and Space Sciences, Washington University, St. Louis, MO 63130, USA. [4]Jet Propulsion Laboratory, California Institute of Technology, Pasadena, CA 91109, USA. [5]Center for Planetary Science, Danish Space Research Institute and Niels Bohr Institute for Astronomy, Physics and Geophysics, University of Copenhagen, Denmark. [6]Space Science Institute, Boulder, CO 80301, USA. [7]Department of Geological Sciences, Arizona State University, Tempe, AZ 85287, USA. [8]Department of Earth, Atmospheric and Planetary Sciences, Massachusetts Institute of Technology, Cambridge, MA 02139, USA. [9]Max Planck Institut für Aeronomie, Katlenburg-Lindau, D-37191, Germany. [10]Institute of Physics and Astronomy, Aarhus University, Aarhus, Denmark. [11]Department of Organismic and Evolutionary Biology, Harvard University, Cambridge, MA 02138, USA. [12]State University of New York, Department of Geosciences, Stony Brook, NY 11794, USA. [13]Department of Earth and Planetary Sciences, University of Tennessee, Knoxville, TN 37996, USA. [14]Astromaterials Research and Exploration Science Office, NASA Johnson Space Center, Houston, TX 77058, USA. [15]DLR Institut fur Raumsimulation, Linder Hoehe, Koln, Germany. [16]NASA Ames Research Center, Moffett Field, CA 94035, USA. [17]Lunar and Planetary Laboratory, University of Arizona, Tucson, AZ 85721, USA. [18]Department of Physics, University of Alabama, Birmingham, AL 35294, USA. [19]Planetary Science Institute, Tucson, AZ 85719, USA.

*To whom correspondence should be addressed. E-mail: kherkenhoff@usgs.gov

spherules, interpreted to be hematitic concretions (*5*), are also found as a relatively resistant component of the outcrops exposed in the walls of Eagle and Fram craters. These observations indicate that the spherules are more resistant to physical and/or chemical erosion than the supporting outcrop matrix. Two other classes of coarse particles are usually present: (i) subangular, irregular particles 1.5 to 5.0 mm in maximum dimension, some with submillimeter circular voids; and (ii) rounded particles 0.5 to 2.0 mm in diameter that are not derived from the spherules or spherule fragments. The irregular particles are probably vesicular basalt fragments, based on their morphology and color (*14*). The rounded particles are often found, along with spherule fragments, within or emerging from a matrix of fine-grained sand and armor ripple bedforms (*6*).

MI images of the soil taken soon after egress show a soil dominated by dark, very fine-grained (<125 μm) particles. Closer to the outcrop, soils contain a greater proportional abundance of spherules. Soils on the opposite side of Eagle crater have more diverse grain populations than those adjacent to the outcrop. The size and shape of the larger grains contained within these soils change considerably over small areas. The cause of these variations is unknown, but wind activity has influenced the distribution of grains within Eagle crater (*14*). MI images taken outside of Eagle crater do not show as much diversity in grain types; spherules, spherule fragments, and dark, very fine sands dominate the soils of the Meridiani plains. There is also a higher fraction of bright material, interpreted to be windblown dust, outside of Eagle crater (*14*).

Surface soil particles imaged by the MI have a generally bimodal size distribution, with grains larger than 1 to 3 mm (very coarse sand to granules) set in a matrix of very fine (<125 μm) sand (*15*, *16*). Whereas the shape of the spherules is primary, other large grains are generally rounded, suggesting abrasion during transport. The bimodal size distribution is inferred to represent wind transport and size sorting, in which the larger grains are moved by surface creep to form a lag, whereas the very fine sands move in saltation (*17*). The paucity of grains intermediate in size between the granules and very fine sand implies either extensive saltation and sorting or a lack of medium-to-coarse sand grains in the source region. The very fine sand grains are more easily moved by wind than the granules, so the coarser grains probably have more local sources than the very fine sand. In contrast to Gusev soils imaged by the MI (*3*), most large grains imaged in Meridiani Planum are relatively free of adhering dust. This observation suggests that very fine sand grains in Meridiani have recently been moved by winds, causing dust removal from grain surfaces. MI images (Fig. 1) suggest that at the surface the fine-grained material is well sorted with a mean grain size in the range of 60 to 150 μm. The lower bound on the size range is uncertain because it is at the MI resolution limit, but the existence of a well-sorted deposit of ~100-μm grains is consistent with predictions of saltation threshold on Mars, because grains of this size are expected to be most easily moved by winds (*18*). However, subsurface soils contain a significant fraction of silt- or clay-size (dust) particles along with a few granules; they are more poorly sorted than the surface materials. Two trenches with maximum depth of ~10 cm were excavated within Eagle crater (*6*). No stratification was observed in the walls of these trenches below the surface layer of well-sorted, very fine sand. When the MB was pressed into the trench bottoms, they were compacted to smooth surfaces (*6*), as would be expected if the soil contained a high proportion of silt- or clay-size particles. In contrast, when the MB was pressed into the dark, fine-grained sand on the surface of the crater floor, much less compaction was apparent (e.g., Fig. 1). These observations suggest that dust particles have been removed from the near-surface layer by winds, concentrating coarser grains that cannot be suspended in the atmosphere (*6*, *14*).

In the investigation of sedimentary rocks exposed in and near Eagle crater, the MI has provided key data that help to integrate observations made by the Panoramic Camera (Pancam) (*19*) with chemical analyses made by the APXS (*11*), MB (*10*), and Miniature Thermal Emission Spectrometer (Mini-TES) (*20*). MI images indicate that outcrop rocks have four principal components: (i) moderately rounded medium to coarse (0.2 to 1 mm) sand grains (probably reworked heterogeneous evaporites—mixtures of sulfates and very fine-grained siliciclastic material) that form mm-scale laminations; (ii) fine-grained and coarser crystalline textures of subsequently precipitated cements and areas of recrystallization; (iii) centimeter-size vugs that record the early diagenetic growth and subsequent dissolution of crystals similar to sulfate crystals in terrestrial evaporites; and (iv) mostly 3- to 5-mm spherules distributed throughout the outcrops. MI images document spatial relationships among these constituents, recording a complex history of deposition and diagenesis. Sandy laminae have been cemented, probably by sulfate minerals, during earliest diagenesis. The large vugs cut across bedding, indicating that the minerals that once filled them also formed diagenetically within the sediments (Fig. 2). Where present, the vugs are found to continue into the rock for at least as deep as the Rock Abrasion Tool (RAT) (*21*) was able to grind (~5 mm) and usually are seen to increase in size with increasing abrasion depth. Accordingly, they are interpreted to represent an intrinsic feature of the outcrops. Vugs exhibit prismatic to discoidal geometry, characteristically with maximum width (1 to 2 mm) near their midpoints and tapering toward their ends. This morphology is consistent with precipitation of certain evaporite minerals within the rock matrix, either displacing or replacing the matrix grains during growth. Vug geometry is most consistent with a monoclinic precursor mineral, analogous to some terrestrial sulfate minerals such as gypsum or kieserite. Subsequently, these minerals were either dissolved by percolating fluid or abraded by wind activity to produce the vugs.

Textural, mineralogical, and compositional features are consistent with the spherules being secondary hematite-cemented concretions formed in a sedimentary sequence, rather than volcanic lapilli or impact glass (*14*, *22*). In particular, MI and Pancam (*19*) images of outcrops show that spherules are not concentrated along depositional bedding planes and thus show no evidence for transport or reworking by physical sedimentary processes

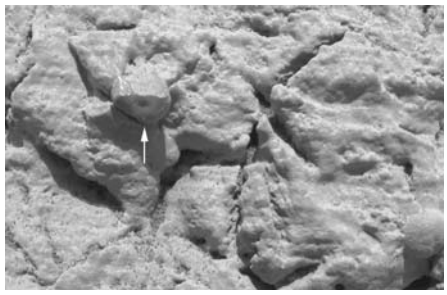

Fig. 2. Part of merge of five MI images of outcrop feature McKittrick (1M130672440 to 1M130672724), taken on sol 28. Illumination is from the top, and the area shown is 2.8 cm across. Concentric banding in the shaded face of a broken spherule is indicated by the arrow. Vugs cut across subhorizontal bedding and are partly filled by dark, very fine sand grains.

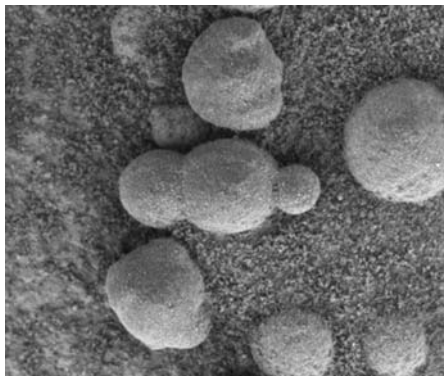

Fig. 3. Part of MI image 1M132444583 of target Tripleberry in the Berry Bowl, taken on sol 48 when the target was in full shadow. The area shown is 1.4 cm across.

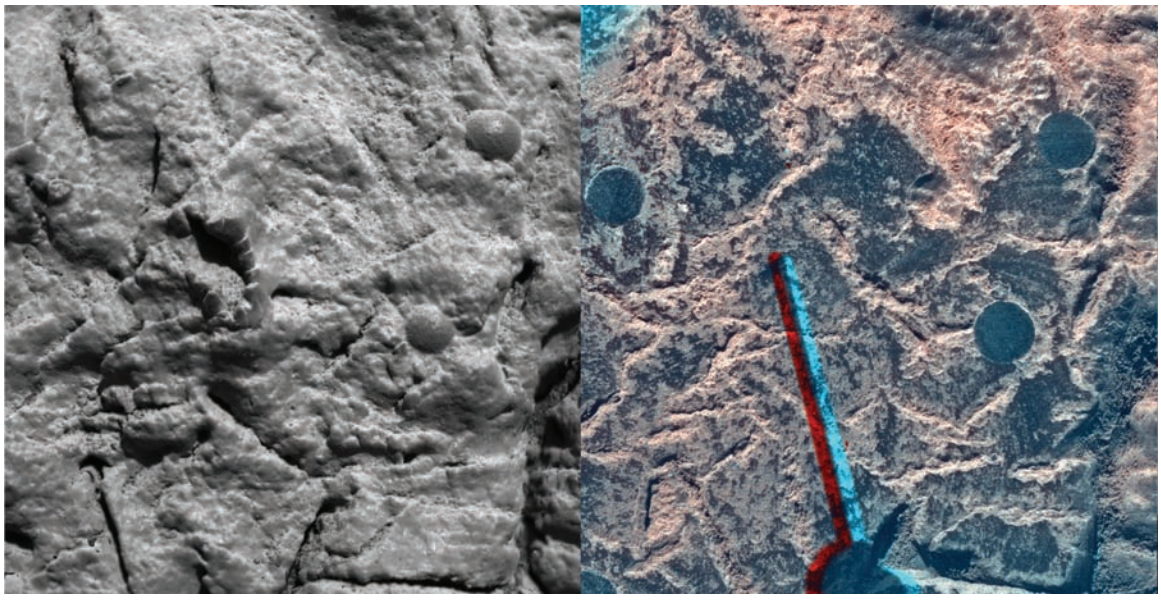

Fig. 4. (**Left**) Merge of three MI images (1M131201538 to 1M131201699) of target King2 on Guadalupe, taken on sol 34 before RAT abrasion. Illumination is from the top, and the area shown is 3 cm across. (**Right**) False-color composite of MI images of the same target on Guadalupe, taken on sol 35 after RAT abrasion. The image taken through the dust cover (1M131296470) is displayed in red, the image taken with the dust cover open (1M131296281) is displayed in green, and the difference (open-closed) is displayed in blue. Red and blue bars are artifacts caused by motion of the shadow of the MI contact sensor between images. Illumination is from the upper left, and the area shown is 3 cm across. Note the lack of internal structure in three abraded spherules (lineations caused by RAT).

(Plates 6 to 10). Bedding is not displaced by spherules, nor are laminae draped over spherules. In rare instances, the spherules form doublets or even triplets aligned along a single axis (Fig. 3). Also, in some cases, in situ spherules have surface grooves parallel to bedding that may reflect minor variations in porosity and permeability among encompassing laminae (*22*). Concretions that impinge into vugs (Fig. 4) and accretionary grooves on concretions that line up with adjacent vugs rather than bedding support the hypothesis that concretionary growth postdated the precipitation of vug precursor crystals. Many spherules show evidence for an increase in the granularity of the matrix immediately adjacent to their margins (Fig. 5), with grains up to a few mm in size sometimes showing radial symmetry around the spherule. This change in granularity might represent a reaction rim, produced as a result of fluid interaction within the adjacent matrix during growth of the spherule. Within the resolving power of the MI (*15*), spherules that are broken or have been cut by the RAT are massive with no internal structure (Fig. 4), except for one broken spherule (Fig. 2) that shows concentric banding (*23*). Spherules are typically polished smooth by the RAT and are harder than the host rock (*6*). The absence of sand textures in the spherules despite formation within a sandy matrix suggests that the primary outcrop grains were soluble and were therefore diagenetically unstable and easily dissolved or recrystallized during concretion growth.

MI images and mosaics provide evidence for the presence of small-scale cross bedding with festoon geometry at Meridiani Planum. An MI mosaic (Plate 6) of part of the outcrop target called Last Chance shows festoon cross-lamination, expressed by lines that dip dominantly to the right, at variable, concave-up angles. Projected into the rock, these lines are contained within dipping planes, which once formed the down-current surfaces of migrating ripples (*22*). The dominance of right over left dips suggests that the outcrop face was oriented at an oblique angle to the current flow direction. In the lower part of Last Chance, the MI mosaic (Plate 6) illustrates several sets of ripple cross-lamination. Cross-laminae dip to the right, indicating that the current that created the cross-lamination was flowing from left to right. A third MI mosaic of a rock called East Dells (Plate 7) reveals abundant small-scale discordant laminae and truncations, including ripple cross-laminae. In a manner similar to that at Last Chance, this rock preserves evidence for festoon ripple cross-lamination, in a view that is largely transverse to current paleoflow. The MI images confirm two key features that lead to the interpretation of water having flowed at times across the surface at the landing site: centimeter-scale cross-stratification and festoon geometry of cross-lamination (*22*).

Bounce rock is an isolated basaltic rock found on the plains of Meridiani southeast of

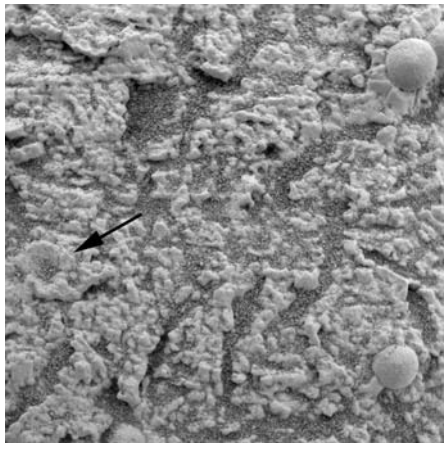

Fig. 5. Merge of five MI images (1M130671710 to 1M130672029) of Algerita outcrop, taken on sol 28 in complete shadow. The area shown is 3 cm across. The arrow indicates a depression, possibly representing the former location of a spherule. Coarser grains (up to ~2 mm) surrounding a spherule can be seen at upper right. The nodular appearance of this outcrop is common in terrestrial evaporites. Dark, very fine sand grains partly fill vugs and other depressions in the outcrop.

Fig. 6. MI image 1M133955069 of target Achsel on Bounce rock, taken on sol 65. Target was in shadow when the image was acquired. Area shown is 3 cm across.

Eagle crater. It may have been ejected by a large, distant impact event. Bounce rock displays an unusual surface texture dominated by polished, parallel striations, ostensibly similar to slickensides formed by differential motion under pressure in terrestrial rocks. The striated surfaces also resemble those found in shatter cones, fracture surfaces commonly found in terrestrial impact structures (*24*). MI images show lineations down to a sub-mm scale and irregular flat surfaces that may be responsible for the rock's specular reflectance (Fig. 6). The MI images further show that these features are limited to a 2- to 3-mm-thick surface that may be differentially resistant to erosion by sandblasting on Meridiani Planum. The rock interior has a rough but predominantly aphanitic texture, with some dark grains that may be phenocrysts. The rock contains mm-scale rounded clasts in exposed fractures and eroded recesses and has been fractured in a pattern that suggests compressional deformation.

References and Notes

1. S. W. Squyres *et al.*, *J. Geophys. Res.* **108**, 8062 10.1029/2003JE002121 (2003).
2. K. E. Herkenhoff *et al.*, *J. Geophys. Res.* **108**, 8065 10.1029/2003JE002076 (2003).
3. K. E. Herkenhoff *et al.*, *Science* **305**, 824 (2004).
4. A martian solar day has a mean period of 24 hours 39 min 35.244 s and is referred to as a sol to distinguish this from a ~3% shorter solar day on Earth.
5. S. W. Squyres *et al.*, *Science* **306**, 1698 (2004).
6. R. E. Arvidson *et al.*, *Science* **306**, 1730 (2004).
7. M. Madsen *et al.*, *J. Geophys. Res.* **108**, 8069, 10.1029/2002JE002029 (2003).
8. The term martian soil is used here to denote any loose, unconsolidated materials that can be distinguished from rocks, bedrock, or strongly cohesive sediments. No implication of the presence or absence of organic materials or living matter is intended.
9. Names have been assigned to geographic features by the MER team for planning and operations purposes. The names are not formally recognized by the International Astronomical Union.
10. G. Klingelhöfer *et al.*, *Science* **306**, 1740 (2004).
11. R. Rieder *et al.*, *Science* **306**, 1746 (2004). Note the abundance of salt-forming elements in soils.
12. G. M. Marion, Special Report 95-12, Cold Regions Research and Engineering Laboratory, U.S. Army Corps of Engineers (1995).
13. W. W. Dickinson, M. R. Rosen, *Geology* **31**, 199 (2003).
14. L. A. Soderblom *et al.*, *Science* **306**, 1723 (2004).
15. The ability to resolve individual grains with the MI depends on the illumination of the scene and the contrast between the grain and its surroundings. Typically, an object must subtend at least 3 pixels to be recognized in an image (about 100 μm for the MI).
16. Grain-size classifications use the Wentworth scale (*25*).
17. An example of a terrestrial eolian lag is shown in figure 6 of Greeley *et al*. (*26*).
18. J. D. Iversen, B. R. White, *Sedimentology* **29**, 111 (1982).
19. J. Bell III *et al.*, *Science* **306**, 1703 (2004).
20. P. R. Christensen *et al.*, *Science* **306**, 1733 (2004).
21. S. Gorevan *et al.*, *J. Geophys. Res.* **108**, 8068, 10.1029/2003JE002061 (2003).
22. S. W. Squyres *et al.*, *Science* **306**, 1709 (2004).
23. Although terrestrial concretions commonly contain internal structures that parallel bedding, this is by no means a ubiquitous or diagnostic feature of concretions; see (*27*).
24. R. S. Dietz, in *Shock Metamorphism of Natural Materials*, B. M. French, N. M. Short, Eds. (Mono-Books, San Francisco, CA, 1968), pp. 267–285.
25. C. K. Wentworth, *J. Geol.* **30**, 377 (1922).
26. R. Greeley *et al.*, *J. Geophys. Res.* **104**, 8573 (1999).
27. J. Sellés-Martínez, *Earth Sci. Rev.* **41**, 177 (1996).
28. The U.S. Geological Survey MER Team developed MI software and created various data products, including some of those displayed in this issue: B. Archinal, J. Barrett, K. Becker, T. Becker, D. Burr, D. Cook, D. Galuszka, T. Hare, A. Howington-Kraus, R. Kirk, E. Lee, B. Redding, M. Rosiek, D. Soltesz, B. Sucharski, T. Sucharski, and J. Torson (project engineer). The Ames MER team and M. Lemmon developed software to merge focal sections and generate anaglyphs from them. The MER Rover Planners provided excellent support of the MI investigation by commanding the instrument arm and MI dust cover. Reviews of this manuscript by J. Bishop, M. Chapman, J. Kargel, and an anonymous referee are much appreciated. This research was carried out for the Jet Propulsion Laboratory, California Institute of Technology, under a contract with the National Aeronautics and Space Administration.

Plates Referenced in Article

www.sciencemag.org/cgi/content/full/306/5702/1727/DC1
Plates 6 to 10

15 September 2004; accepted 9 November 2004

REPORT

Localization and Physical Property Experiments Conducted by Opportunity at Meridiani Planum

R. E. Arvidson,[1]* R. C. Anderson,[2] P. Bartlett,[3] J. F. Bell III,[4] P. R. Christensen,[5] P. Chu,[3] K. Davis,[3] B. L. Ehlmann,[1] M. P. Golombek,[2] S. Gorevan,[3] E. A. Guinness,[1] A. F. C. Haldemann,[2] K. E. Herkenhoff,[6] G. Landis,[7] R. Li,[8] R. Lindemann,[2] D. W. Ming,[9] T. Myrick,[3] T. Parker,[2] L. Richter,[10] F. P. Seelos IV,[1] L. A. Soderblom,[6] S. W. Squyres,[4] R. J. Sullivan,[4] J. Wilson[3]

The location of the Opportunity landing site was determined to better than 10-m absolute accuracy from analyses of radio tracking data. We determined Rover locations during traverses with an error as small as several centimeters using engineering telemetry and overlapping images. Topographic profiles generated from rover data show that the plains are very smooth from meter- to centimeter-length scales, consistent with analyses of orbital observations. Solar cell output decreased because of the deposition of airborne dust on the panels. The lack of dust-covered surfaces on Meridiani Planum indicates that high velocity winds must remove this material on a continuing basis. The low mechanical strength of the evaporitic rocks as determined from grinding experiments, and the abundance of coarse-grained surface particles argue for differential erosion of Meridiani Planum.

The Mars Exploration Rover (MER) Mission required accurate tracking of the location of Opportunity to ensure efficient drives and to place measurements in proper geological context, e.g., associating a rock target with a particular terrain or geologic unit (*1*–*3*). The location of the lander in inertial coordinates was determined by fitting direct-to-Earth, two-way, X-band Doppler radio transmissions and two passes of two-way Ultra High Frequency (UHF) Doppler transmissions between Opportunity and the Mars Odyssey Orbiter. Based on analyses of these observations, the landed location is 1.9483°S (with an accuracy of ~10 m) and 354.47417°E (with an accuracy of ~10 cm), translated to International Astronomical Union (IAU) 2000 areocentric coordinates. The landed location was also tied to Mars Global Surveyor (MGS) Mars Orbital Camera and MER descent image data to within ~10-m accuracy, by triangulation to three craters observed in the far field [through breaks in the local Eagle crater rim (*4*)] in Pancam images. These triangulation results, mapped to the cartographic network–derived MGS Mars Orbital Laser (MOLA) data (*5*), imply that the lander is located at 1.9462°S, 354.4734°E in IAU 2000 areocentric coordinates.

Opportunity stopped on the plains for a software upload on sols 75 to 78 (*6*), and its location (1.94752°S, 354.47716°E) was determined by analysis of two passes of UHF two-way Doppler tracking. The location was also determined by image-based triangulation to common features, with resultant values of 1.9453°S, 354.4766°E. For both landing and software-upload locations, the Doppler-based location was displaced 135 m